

This discussion paper is/has been under review for the journal Atmospheric Measurement Techniques (AMT). Please refer to the corresponding final paper in AMT if available.

Characteristics of cloud liquid water path from SEVIRI on the Meteosat Second Generation 2 satellite for several cloud types

A. Kniffka¹, M. Stengel¹, M. Lockhoff¹, R. Bennartz², and R. Hollmann¹

¹Satellite-based Climate Monitoring, Deutscher Wetterdienst, Strahlenbergerstr. 13, 63067 Offenbach, Germany

²University of Wisconsin – Madison, 1225 W. Dayton St., Madison, WI 53706, USA

Received: 3 July 2013 – Accepted: 17 September 2013 – Published: 2 October 2013

Correspondence to: A. Kniffka (anke.kniffka@dwd.de)

Published by Copernicus Publications on behalf of the European Geosciences Union.

Title Page

Abstract

Introduction

Conclusions

References

Tables

Figures

◀

▶

◀

▶

Back

Close

Full Screen / Esc

Printer-friendly Version

Interactive Discussion



Abstract

In this study the temporal and spatial characteristics of liquid water path (LWP) of low, middle level and high clouds are analysed using space-based observations of the Spinning Enhanced Visible and Infrared Imager (SEVIRI) onboard the Meteosat Second Generation 2 (MSG2) satellite. Both geophysical quantities are part of the dataset CLAAS (CLOUD property dAtAset using SEVIRI) and are generated by EUMETSAT's Satellite Application Facility on Climate Monitoring (CM SAF). In this article we focus on the statistical properties of LWP retrieved at daylight associated with the individual cloud type. Our results reveal that each cloud type possesses a characteristic LWP distribution. These frequency distributions are constant with time in the entire SEVIRI field of view, but vary for smaller regions like Central Europe. The average LWP is higher over land than over sea, in case of low clouds 15–27 % for 2009 and the variance of the frequency distributions is enhanced. Also, the average diurnal cycle of LWP is related to cloud type where most pronounced diurnal variations were detected for middle level clouds. With SEVIRI it is possible to distinguish between intrinsic LWP variability and variations driven by cloud amount. The relative amplitude of the intrinsic diurnal cycle can exceed the cloud amount driven amplitude.

1 Introduction

An essential parameter for monitoring climate variability is the large scale view of cloud field distribution. Clouds influence strongly the energy budget and water cycle of the Earth and have therefore a major impact on the atmospheric state at shorter time periods as well as climatic relevant timescales. Due to their complexity in both formation mechanisms as well as spatial and temporal variability, the knowledge about many cloud aspects is limited. In a recent comparison of General Circulation Models the consistency with observations differs strongly among the models. Particularly low clouds account much for the climate sensitivity in the considered models (Williams

AMTD

6, 8743–8782, 2013

LWP and CTY

A. Kniffka et al.

Title Page

Abstract

Introduction

Conclusions

References

Tables

Figures

⏪

⏩

◀

▶

Back

Close

Full Screen / Esc

Printer-friendly Version

Interactive Discussion



LWP and CTY

A. Kniffka et al.

Title Page

Abstract

Introduction

Conclusions

References

Tables

Figures

◀

▶

◀

▶

Back

Close

Full Screen / Esc

Printer-friendly Version

Interactive Discussion



and Webb, 2009). Bony and Dufresne (2005) studied in detail the tropical cloud evolution in General Circulation Models and suggest the representation of marine boundary layer clouds is the main source of uncertainty in tropical cloud feedbacks simulated by the models. Satellite data can help to improve our understanding, amongst others by serving as input for climate models or numerical weather prediction models. Jiang et al. (2013) intercompared 19 climate models in the Cloud model Intercomparison Project (CMIP). They documented the improvement of the description of column-integrated cloud amount in more than half of the models from Phase 3 to Phase 5 of the project. Chlond et al. (2004) modelled the liquid water path of marine clouds with Large Eddy Simulation and Single Column Models and state, that clouds remain the largest uncertainty for assessing the impact of anthropogenic influence on climate change. Naturally, cloud's complexity is not only a challenge for modelling but also for retrieving via radiance measurements from satellite. The intercomparability is explored for example in the Global Energy and Water Cycle Experiment, see Stubenrauch et al. (2009). Measured brightness temperatures and reflectance impacted by clouds depend strongly on their macro- and microphysical characteristics like cloud amount and cloud top height, as well as droplet size distribution, texture and thermodynamic phase. They are also affected by the atmospheric conditions and by the sun and satellite respective positions. Having a good knowledge of these conditions and positions allows the retrieval of cloud properties from the remaining signal.

The diurnal or daytime cycle of satellite-derived LWP has been well documented in several studies (Wood et al., 2002; O'Dell et al., 2008; Painemal et al., 2012), in detail mainly for specific regions such as the west coast of South America (Painemal et al., 2012). In our study, we go beyond these and analyse and discuss the relationship between cloud type and liquid water path as they are categorised by CM SAF. Both variables are derived from the Spinning Enhanced Visible and Infrared Imager (SEVIRI) onboard the Meteosat Second Generation 2 (MSG2) satellite. Characteristic features of LWP concerning its distribution and diurnal cycle for the individual cloud types are explored. The results of the one year time-frame are put into context with

LWP and CTY

A. Kniffka et al.

Title Page

Abstract

Introduction

Conclusions

References

Tables

Figures

◀

▶

◀

▶

Back

Close

Full Screen / Esc

Printer-friendly Version

Interactive Discussion



the University of Wisconsin (UWisc) cloud liquid water path climatology derived from 18 yr of passive microwave observations, see O'Dell et al. (2008). The general features of LWP, for example frequency distribution, average value and diurnal cycle are specified to serve as characteristic measures in atmospheric numerical modelling. More specifically, they can be used to conduct process studies, assist in the evaluation of microphysical measurement experiments such as airborne probing of clouds and serve as input for cloud generators and radiative transfer studies on a wide range of spatial scales. The temporal resolution of MSG2 permits assessing the temporal evolution of cloud systems in cloud resolving models and facilitate model evaluation studies such as undertaken in Hanay et al. (2009), Brunke et al. (2010) or the above mentioned.

The article is structured as follows: in Sect. 2 the methods of LWP and CTY (cloud type) retrieval from SEVIRI measurements are described, Sect. 3 contains the analysis of LWP with respect to CTY, where the statistical properties are considered first, followed by a subsection on liquid water in high opaque clouds. The analysis is completed with a consideration of LWP diurnal cycle for several regions and a comparison with the climatology of microwave-based LWP observations (O'Dell, 2008). Also the seasonal variations for the considered year are presented in a subsection. In Sect. 4 the results are discussed taking into account the limitations of a geostationary imager.

2 Generation of LWP and CTY from SEVIRI measurements

In this study, non-averaged data of LWP and CTY derived from SEVIRI measurements form the data basis. Both parameters are part of the dataset CLAAS (CLOUD property dAtaset Using SEVIRI) by CM SAF (Schulz et al., 2009) that includes cloud micro- and macrophysical properties as well as surface albedo and spans the time period 2004–2011. The radiances were measured with the passive optical imaging radiometer SEVIRI. It is equipped with 12 spectral channels at visible and infrared wavebands. SEVIRI is mounted on the geostationary MSG satellites, where MSG 1 and MSG 2 measurements were projected so that the subsatellite point appears to be $0^{\circ}/0^{\circ}$ while they are

[Title Page](#)[Abstract](#)[Introduction](#)[Conclusions](#)[References](#)[Tables](#)[Figures](#)[Back](#)[Close](#)[Full Screen / Esc](#)[Printer-friendly Version](#)[Interactive Discussion](#)

the illumination, the conditions can be twilight or daylight and night time. Also the geographical location, the viewing geometry, the water vapour content and a coarse atmospheric structure are taken into account, where the latter two are both described by numerical weather prediction data. As input vertical profiles of temperature and humidity as well as water vapour content from ERA interim were used. ERA interim is a global reanalysis and is produced within the ERA reanalysis project of the European Centre for Medium-Range Weather Forecasts (Dee et al., 2011). As a first step, pixel with semitransparent or fractional clouds are identified, after that the low, middle and high cloud classification is performed by using a threshold for the brightness temperature of the $10.8\ \mu\text{m}$ channel that is related to the cloud top height. ERA interim analysis temperatures at several pressure levels are used to compute the thresholds that allow to separate very low from low clouds, low from medium high clouds and so on. From statistical analysis of the cloud top pressure, that is assigned afterwards, five cloud top pressure ranges for the different cloud types resulted that are listed in Table 1. For cloud type and pressure as well as cloud liquid water path NWC SAF's cloud mask is used as input. A type is only derived for a pixel that was masked to be completely cloudy. Pixel with inherent sub-pixel cloudiness are ascribed to the fractional cloud class without further testing.

From the cloud type algorithm 15 carefully defined cloud types result; CM SAF groups these types into 5 more general classes which are: low clouds, middle level clouds, high opaque, high semitransparent and fractional clouds. Usually the latter step is done during the spatial and temporal averaging procedure, but since in this study the non-averaged (level 2) data were analysed, the reclassification was done directly after the CTY-algorithm.

Evaluation of the cloud type product is carried out by CM SAF as described in Hollmann (2011). Here the cloud type product from two sensors, SEVIRI and AVHRR (Advanced Very High Resolution Radiometer) is compared. Since the cloud type classes are not completely equal for the two sensors, two artificial classes are generated, to reduce the data to the least common denominator: high clouds and cirrus clouds. The

[Title Page](#)[Abstract](#)[Introduction](#)[Conclusions](#)[References](#)[Tables](#)[Figures](#)[⏪](#)[⏩](#)[◀](#)[▶](#)[Back](#)[Close](#)[Full Screen / Esc](#)[Printer-friendly Version](#)[Interactive Discussion](#)

time series of AVHRR and SEVIRI-based products resemble each other closely in case of high clouds, though it has to be noted, that even with the generation of the artificial classes the two products are not completely based on the same conditions. Both products are also compared against MODIS which shows 10–20 % smaller values (% is to be understood in absolute units, i.e. 10 % cloud fraction of type x). This could be expected, because MODIS “High clouds IR” category defines all clouds detected above 400 hPa, while for the corresponding CM SAF products the reference level is 500 hPa. Also the cirrus clouds class is compared against MODIS, for the SEVIRI product differences between 10–20 % occur, where MODIS gives a higher fraction. These can partly be explained by the differences in the reference thresholds for MODIS and SEVIRI, leading to more observed clouds with the MODIS instrument, but naturally high and thin clouds can be more reliably detected with a spectrally and spatially higher resolved instrument.

For a typical CTY-field with liquid water and ice pixel on the SEVIRI field of view, also called SEVIRI disc, see Fig. 1 on the left hand side. In this snapshot all cloud types are present, at the same time low and high opaque clouds dominate most of the cloudy regions. The corresponding LWP-values are displayed on the right hand-side. The LWP-field covers a smaller region due to the restriction of both, the viewing zenith angle and the solar zenith angle being smaller than 72° (Stengel et al., 2013). Also note that particularly in the tropical regions the cloudy pixel are often icy on top, in this figure they are not displayed because of the restriction to liquid water. Highest values for LWP can be found mainly in cloud bands with high opaque clouds, but also low and middle level clouds can be associated by the retrieval algorithms with high LWP values, e.g. middle Europe.

2.2 Cloud liquid water path derivation

For consistency reasons, CPP v3.9 makes use of the cloud-mask processed beforehand. In principle, the retrieval method relies on the assumption that cloud reflectance and so SEVIRI’s visible channels are mainly influenced by the cloud’s optical thickness

LWP and CTY

A. Kniffka et al.

Title Page

Abstract

Introduction

Conclusions

References

Tables

Figures

◀

▶

◀

▶

Back

Close

Full Screen / Esc

Printer-friendly Version

Interactive Discussion



(τ), whereas changes in the infrared depend on the effective radius (r_{eff}) of the cloud droplets. The $0.6\ \mu\text{m}$ channel and the $1.6\ \mu\text{m}$ channel proved to deliver the most accurate results. τ and r_{eff} are determined by comparing simultaneously the radiances for the 2 channels with radiances in look-up tables for various values of τ and r_{eff} . The look-up tables were generated with the Doubling-Adding KNMI (DAK) radiative transfer model, which makes use of a doubling-adding method (De Haan et al., 1987) and Stammes (2001). In the model, clouds are assumed to be plan-parallel and horizontally homogeneous and they are embedded in a vertically stratified medium allowing for Rayleigh scattering. Surface albedo is assumed to have a constant value of 0.1 over land and 0.05 over ocean for $0.6\ \mu\text{m}$ as well as 1.5 and 0.05 for the $1.6\ \mu\text{m}$ channel. The droplets themselves are assumed to be spheres with effective radii between 1 and $24\ \mu\text{m}$ and an effective variance of 0.15 in their gamma type distribution. The cloud liquid water path is finally retrieved via the relation (Stephens, 1978):

$$\text{LWP} = \frac{2}{3} \tau r_{\text{eff}} \rho \quad (1)$$

with ρ being the density of liquid water. The retrieved particle size values are unreliable for optically thin clouds and so for clouds with cloud optical thickness $\text{COT} < 8$ the climatological value $8\ \mu\text{m}$ is used, which is similar to values used by Rossow and Schiffer (1999).

Roebeling et al. (2008) validated the retrieved LWP values with CloudNET data from two measurement sites: Chilbolton and Palaiseau. At the two sites, measurements were taken with microwave radiometers (MWR). One year of MWR-retrieved values was compared to the SEVIRI LWP values, retrieved with the algorithm outlined above. The derived accuracy is variable and depends on a number of factors, mainly viewing geometry, collocation uncertainties and inhomogeneity of clouds. For summer months, daily and monthly derived LWP values agreed within $5\ \text{g m}^{-2}$, corresponding to a relative accuracy of 10%. In winter, the accuracy was found to be $10\ \text{g m}^{-2}$, which was caused by the unfavourable viewing geometry and the smaller amount of data values.

The diurnal variations of SEVIRI-derived LWP did not differ more than 5 g m^{-2} from the MWR-measurements.

The dataset CLAAS itself has undergone a careful validation process, whose results are documented in the validation report of CM SAF (Kniffka et al., 2013). The non-averaged cloud phase was validated on pixel basis with CALIOP on CALIPSO (Cloud-Aerosol Lidar with Orthogonal Polarization on Cloud-Aerosol Lidar and Infrared Pathfinder Satellite Observations), monthly mean values of the complete time series of LWP and CPH (cloud phase) were validated against MODIS. LWP was also compared against MODIS on non-averaged pixel basis.

The 8 yr cloud phase time-series of CLAAS was compared to the Modis Optical and the MODIS Infrared dataset (Meirink et al., 2013b), it agrees generally with both, but best with the MODIS-IR product. When studying the spatial patterns, differences in the higher liquid cloud fraction over the tropical land and the lower liquid cloud fraction in the Sahara and at high solar zenith angles can be noticed.

The liquid water path time-series of CLAAS and MODIS are in very good agreement, particularly the seasonal cycle is nearly identical. The spatial patterns that are produced by MODIS and SEVIRI are in good agreement, though differences can be found in regions with strongly broken cloud cover (e.g. the South-Atlantic trade cumulus region), where the algorithms have different treatment of clear-sky restoral and the pixel resolution has a great effect. CPH, LWP and cloud fractional cover including CTY meet the requirements for a qualified dataset of the CM SAF project (Kniffka et al., 2013b).

3 Analysis

This analysis is based on level 2 datasets of CTY and LWP, with CPH as auxiliary data. Four months of 2009 were analysed instead of averaging over a complete year in order to highlight the effect of the individual seasons. In the following, only those pixel, that were marked as filled with liquid water were considered; ice or mixed phase

Title Page

Abstract

Introduction

Conclusions

References

Tables

Figures

◀

▶

◀

▶

Back

Close

Full Screen / Esc

Printer-friendly Version

Interactive Discussion



[Title Page](#)[Abstract](#)[Introduction](#)[Conclusions](#)[References](#)[Tables](#)[Figures](#)[⏪](#)[⏩](#)[◀](#)[▶](#)[Back](#)[Close](#)[Full Screen / Esc](#)[Printer-friendly Version](#)[Interactive Discussion](#)

was excluded from the discussion. The analysis was restricted to liquid cases since the two branches of liquid and ice retrieval in the CPP algorithm are not comparable. Ice crystals have a larger variety in shapes, hexagons and clustered pieces in various forms as opposed to mere spherical liquid droplets. Therefore more assumptions have to be made concerning the shape of the particles in the retrieval of ice water content.

All cases refer to the intrinsic variability of LWP. This means we have only LWP-filled pixel taken into account to eliminate the effect of changes in cloud fractional cover (CFC) in e.g. the diurnal cycle of LWP. The comparison with the LWP climatology of O'Dell (2008) is an exception for the sake of comparability. Here we also took the chance to demonstrate CFC and LWP diurnal fluctuations for a predefined region.

3.1 General characteristics of distributions and statistical properties

One objective of the present study was to explore the potential for parameterisation of LWP in relation to CTY suitable for process studies or model evaluation and testing. From each pair of LWP and CTY fields frequency distributions of LWP were determined for the individual cloud types, where the pixel were sorted with respect to local time. It was found that the shape of the frequency distributions themselves remained constant with time, in case a larger area is considered. Bugliaro et al. (2011) evaluated the cloud property retrievals used by CM SAF with simulated satellite radiances based on the output of the COSMO-EU weather model. It was found that CM SAF's algorithms are capable of reproducing the real LWP distribution concerning the form (modal classes and skewness), with a slight overestimation of the histogram peak location and an underestimation of the peak number of occurrences in the considered test data set.

The distributions for all points in time and all cloud types are unimodal and positively skewed. With these constant properties it is possible to characterise a cloud type with a certain distribution possessing characteristic parameters. For a mathematical description either a lognormal distribution or a gamma type distribution has to be chosen. The skewness that is unequal 0 forbids description with the help of a Gaussian distribution. This corresponds to the findings of de la Torre Juárez et al. (2011) who

LWP and CTY

A. Kniffka et al.

Title Page

Abstract

Introduction

Conclusions

References

Tables

Figures

◀

▶

◀

▶

Back

Close

Full Screen / Esc

Printer-friendly Version

Interactive Discussion



derived fitting functions for the probability distributions of LWP amongst other cloud properties retrieved from MODIS-Aqua. In their work, the best fit was found to be either lognormal or gamma type, depending on the considered spatial scale. Unlike in Con-
sidine et al. (1997), who proposed gaussian distributions in case of very large cloud
fractions close to 100 %, a gaussian distribution was never the best fit. The gamma
type distribution is also detectable from ship-based as well as airborne measurements
(McBride et al., 2012).

In general, the distributions can be characterised as such (see also Fig. 2): low
clouds show on average a rather narrow highly peaked distribution with small liquid
water contents of approximately $67.2\text{--}86.2\text{ g m}^{-2}$. The averaged variance ranges from
21.9 to 29.7 g m^{-2} .

Middle level clouds possess a larger spectrum of LWP, the average values are be-
tween 153.8 g m^{-2} in July and 174.8 g m^{-2} in October while the variance lays between
 51.5 g m^{-2} in April and 58.1 g m^{-2} in January.

The distributions with highest absolute values can be found in the high opaque cloud
class, at the same time the distribution is not as broad as for middle level clouds. The
average values range for this class from 148.8 g m^{-2} in January up to 187.3 g m^{-2} in
April. The variance changes between 50.3 g m^{-2} in October and 59.2 g m^{-2} in July.
High semi-transparent clouds again have smaller average values compared to the high
opaque class (34.4 g m^{-2} in April – 43.9 g m^{-2} in October) and the most narrow distri-
butions of all (variance: 11.0 g m^{-2} in April – 16.0 g m^{-2} in January). More figures on
averages and variances for the complete MSG disc as well as a subset for Europe can
be found in Table 3.

As a next step, let us consider specified regions. A distinction between land and
water pixels leads to the following observations: distributions appear broader for land
pixel than for water pixel, this means, the variance is greater and more high LWP val-
ues are measured. On average LWP is higher over land than over sea: for example low
clouds show the following behaviour: in January 98.8 g m^{-2} compared to 84.0 g m^{-2} ,
April: 78.4 g m^{-2} and 65.4 g m^{-2} , July: 79.3 g m^{-2} , 63.4 g m^{-2} , October: 108.6 g m^{-2} ,

LWP and CTY

A. Kniffka et al.

Title Page

Abstract

Introduction

Conclusions

References

Tables

Figures

◀

▶

◀

▶

Back

Close

Full Screen / Esc

Printer-friendly Version

Interactive Discussion



cloud class fraction increases to exceed the high semitransparent one. In Europe, the monthly variation for all cloud types is generally bigger compared to the results for the full SEVIRI disc. Most noticeable is the increase in fractional clouds during the summer months which is not visible when considering the full disc and the subsequent raise of the high opaque cloud class from September to December. This might indicate that the raise is merely caused by seasonal changes in the circulation pattern. A shift of the general circulation like the meridional movement of the polar front has an observable effect in this small subset of the SEVIRI disc. The differences become much more noticeable when considering smaller time-scales. For October 2009 daily averages of LWP were calculated from the non-averaged data for the respective European region. The average is a daylight-only average, where the illuminated hours were taken as weighting factor. The time series for low clouds is displayed in the upper panel in Fig. 4 together with the daily averages. The time series shows a pronounced temporal variation with apparently periodic fluctuations. The repetition period is in the order of several days, which corresponds to the time scale of synoptic features such as cyclones and anticyclones. The auto-correlation function reveals, that the fluctuations solely appear to be periodic, which can be expected for a single month of data within a chaotic dynamic system. As can be seen from Table 3, the monthly mean values show for middle level and high opaque clouds on average enhanced LWP values, on the contrary the LWP of the high semitransparent and the fractional cloud class is smaller in Europe, compared to the full SEVIRI disc. A typical uncertainty is caused by the viewing geometry of SEVIRI since it is mounted on a geostationary satellite: the cloud amount and also the liquid water path are dependent on the line of sight through the atmosphere, and so the error increases towards the rims of the disc, see the Validation Report for CLAAS (Kniffka et al., 2013).

The connection between high-semitransparent clouds and liquid water can only be rated as approximate, because of an inconsistency between cloud top temperature (CTT) from the msgv2012 algorithm and the one used for the derivation of the cloud physical properties. In CPP v3.9, the cloud top temperature is derived from the 10.8 μm

LWP and CTY

A. Kniffka et al.

Title Page

Abstract

Introduction

Conclusions

References

Tables

Figures



Back

Close

Full Screen / Esc

Printer-friendly Version

Interactive Discussion



the existence of large amounts of liquid water also in great heights up to 9 to 10 km seems to be a common feature of deep vigorous convective clouds, but is not often modelled by cloud modellers due to gaps in knowledge and lack of parameterisations for some microphysical processes. Particularly the rate of drop freezing seems to be overestimated significantly, mostly in the temperature range from -32 to -38 °C.

Another question arises when dealing with multi-algorithm data: could the cloud phase attached to the cloudy pixels that were identified as e.g. high opaque, be erroneous? Both quantities are derived with different algorithms and therewith inconsistent in a numerical sense, so it might be possible, that the phase “liquid” is attached falsely to a cloudy pixel. Also the number of high clouds that are flagged as liquid is fairly small compared to the other cloud types. To make our results more plausible, we restricted the fields for October 2009 with the corresponding cloud top temperature (CTT). Pixel with liquid phase and cloudy were only considered to be valid if the cloud top temperature was greater than -38 °C. We found that the pixels are not randomly distributed, but form contiguous areas. Also the pixels are not preferably situated in regions with high viewing angles, where the detection of clouds becomes more complicated, due to the slant viewing geometry. High opaque liquid cloud pixels are found both over water as well as over land, as can be seen in the cloudy regions in Fig. 5. On the left hand side the pixels lay over water, on the right hand side the cloudy patches can be found both over water and over land. In this figure, only pixels with the above described conditions are displayed plus the restriction of $CTT > -38$ °C. No dependence on the underlying surface could be found.

The number of pixels with high opaque clouds and liquid water and $CTT > -38$ °C is much smaller compared to other cloud types at the same conditions. When averaging the data for October 2009, the cloudy pixels belonging to the conditions above consist of 87.3% low clouds, 3.6% middle level clouds, 0.24% high opaque clouds and 8.8% high semitransparent clouds. So the number of high opaque pixels is approximately 7% of the number of middle level clouds. Still the number is not negligible, and approves the findings of Khain et al. (2001). A more detailed analysis of this subject

[Title Page](#)[Abstract](#)[Introduction](#)[Conclusions](#)[References](#)[Tables](#)[Figures](#)[Back](#)[Close](#)[Full Screen / Esc](#)[Printer-friendly Version](#)[Interactive Discussion](#)

can be found in Hogan et al. (2004). The authors measured the global distribution of supercooled water clouds by analysing data from the Lidar In-space Technology Experiment (LITE). The lidar mounted on a space shuttle had the advantage of providing a view from above, as a satellite instrument does and so delivers results that are suitable for comparison with our data. In this study, the highest amounts of the coldest supercooled clouds were found in the midlatitudes of the northern and Southern Hemisphere, but not in the region of the Inter-Tropical Convergence Zone. Also Hu et al. (2010), who studied the occurrence of supercooled water clouds with CALIPSO found supercooled clouds mainly in mid- or high-latitudes, associated with storm-track regions. This corresponds roughly to our findings for October 2009, but a more careful study with a broader database would have to be made.

3.2 Diurnal cycle

Directly from the level2 data, monthly averaged diurnal cycles of LWP were created per cloud type for the Northern Hemisphere of the SEVIRI disc. The local time of the individual data points was taken into account by sorting the pixel into time zones. In Fig. 6 the results for October 2009 are displayed, it needs to be aware that the algorithm yields results during daylight only. LWP shows diurnal variations for all cloud types, whereat the middle level cloud type has the biggest amplitude. The LWP of low clouds shows maximal values in the morning hours and around midday, whereas middle level clouds peak in the afternoon (local time). The diurnal amplitude of low clouds is very pronounced, not only in October, on average it reaches 29.1 % of the mean LWP and at maximum 56 % of the mean LWP value (April). Pfeifroth (2009) analysed the diurnal variation of cloud fractional cover from SEVIRI as it is generated by CM SAF for the year 2008 and found that the average CFC has a relative diurnal cycle of less than 30 % from the average CFC for 58.5 % of all considered pixel. In relative terms, this indicates that LWP can be more variable than the cloud fraction from SEVIRI during a day! LWP and CFC fluctuations cannot be compared directly, CFC fluctuations for example result only from variation in horizontal direction, whereas LWP can vary in three dimensions.

LWP and CTY

A. Kniffka et al.

Title Page

Abstract

Introduction

Conclusions

References

Tables

Figures

◀

▶

◀

▶

Back

Close

Full Screen / Esc

Printer-friendly Version

Interactive Discussion



Nevertheless both kinds of fluctuation cause variations in cloud optical thickness which again influences the radiative budget. Fluctuations in COT for different reasons could directly be compared. Further studies are required to confirm the observations and to analyse the effect on cloud optical thickness or the radiative budget, respectively.

In Fig. 6, also the number of observations is depicted, to illustrate the dependence of the CPP algorithm on the illumination conditions. For solar zenith angles above 72° no useful information can be retrieved for the liquid water path and so in conjunction with the viewing geometry of geostationary MSG2 the number of observations is mainly dependent on the time of day.

Marine boundary layer clouds are a major source of uncertainty in cloud radiative feedback, as stated in several publications, see Chlond et al. (2004), Seethala and Horváth (2010) or Wood and Hartmann (2006). Therefore, the climate modelling community would greatly benefit from accurate LWP measurements of marine boundary layer clouds. Since those clouds are relatively optically thin, their radiative impact is very sensitive to their vertically integrated liquid water content or liquid water path (Turner et al., 2007). The cloud deck off the coast of Africa, approximately at Namibia and Angola serves as an example for marine boundary layer clouds that consist mainly of water. This special region shall be considered in more detail. Therefore, a field between 5°W – 15°E and 30°S – 10°S was cut from the MSG data (compare Fig. 1) for LWP and CTY and the level 2 data from the months January, April, July and October were averaged to form monthly mean diurnal cycles for the respective cloud types.

In Fig. 7 the average diurnal cycle of low and middle level clouds for the cloud deck is shown. As can be seen on the left hand side, the diurnal cycle of low clouds shows a strong morning maximum, tends to decrease during the day and then raise again around 02:00 LT. This is valid for the months January, April, July and October. A course of this type is caused by solar absorption where the cloud cover is heated during daytime which leads to the evaporation of cloud droplets and thinning of the cloud cover. This effect can be simulated for example with a Large Eddy Simulation Model by including shortwave-heating (Chlond, 2004). Wood et al. (2002) propose fitting coefficients

LWP and CTY

A. Kniffka et al.

[Title Page](#)[Abstract](#)[Introduction](#)[Conclusions](#)[References](#)[Tables](#)[Figures](#)[Back](#)[Close](#)[Full Screen / Esc](#)[Printer-friendly Version](#)[Interactive Discussion](#)

for the diurnal cycle of LWP for low clouds which agree with our findings. These fitting coefficients to a sinusoidal curve were derived from microwave radiometer data of TMI (Tropical Rainfall Measuring Mission Microwave Imager). The middle level clouds on the right hand side do not show such a constant shape of diurnal cycle, in January and April the maximal value is reached in the early afternoon, whereas in July and October the maximal values appear in the morning, but no pronounced maximum can be observed.

In these considerations we have to take into account, that it is possible for clouds to develop during a day, for example through convection and change the cloud type class. To illustrate this effect, we analysed this special region which should provide a temporally stable cloud layer. Stable is meant in a sense that this layer stays in more or less the same geographic location in the time frame of a month. Hence the observed changes in CTY and LWP should result mainly due to internal developments of the cloud deck during daytime. In Fig. 8 the average diurnal cycle of LWP together with the number of observations is displayed for the cloud deck in April 2009. The LWP of low clouds is highest in the morning hours and decreases during daytime, also the number of observed low clouds decreases until 12:00 UTC and increases afterwards. The numbers of middle level and high semitransparent clouds show a similar development. At the same time the number of fractional clouds increases to reach a maximum at 11:00 UTC, plus the number of high opaque clouds increases until 10:00 UTC before decreasing again. Because of the spatial stationarity of the considered cloud deck, this indicates a transition of clouds from one type to another in this region. We are aware that this study can give only a rough impression on the possibility of cloud class transition and that temporally and spatially much higher resolved analysis would be needed to make a more quantitative declaration for this specific region.

For further characterisation, the diurnal cycles of LWP derived from SEVIRI were compared to climatological diurnal cycles derived from passive microwave observations (O'Dell et al., 2008). From this climatology a small subset was processed for our region specified above. In Fig. 9 a direct comparison between the SEVIRI derived LWP

LWP and CTY

A. Kniffka et al.

[Title Page](#)[Abstract](#)[Introduction](#)[Conclusions](#)[References](#)[Tables](#)[Figures](#)[⏪](#)[⏩](#)[◀](#)[▶](#)[Back](#)[Close](#)[Full Screen / Esc](#)[Printer-friendly Version](#)[Interactive Discussion](#)

values and the microwave measurements (aggregated from SSM/I, TMI and AMSR-E data) can be found. The microwave data are climatological average values from the years 1988–2008, the SEVIRI data are monthly averages from the year 2009. For a better comparability also cloud-free pixel were averaged and no distinction between cloud types was made, though clouds in this region are mostly of low type. As can be seen, the shape of the diurnal cycles derived from SEVIRI corresponds well with the diurnal cycles derived from the climatology, particularly April and July show a good agreement. The absolute values from the SEVIRI measurements are higher for all months. As can be seen on the right hand side of Fig. 9 it is possible to provide also temporally resolved diurnal cycles with SEVIRI, so also the temporal fluctuation of the diurnal cycle can be studied as opposed to measurements from polar orbiting instruments.

The diurnal cycle of LWP can be caused by either the intrinsic fluctuations of LWP within a cloud field or by the macroscopic change of cloud cover, which means absence or presence of clouds in this respect. In Fig. 10 we refined the diurnal cycle description by splitting the average diurnal cycle into these two parts. The intrinsic share is determined by averaging over all pixel with $LWP > 0.0 \text{ g m}^{-2}$. The macroscopic change in cloud cover is assessed by creating masks with the entry 1 for pixel with $LWP > 0.0 \text{ g m}^{-2}$ and 0 for pixel without clouds or with ice, subsequently the average is formed by including all pixel in the mask. For a better comparability, the resulting diurnal cycles are displayed in Fig. 10 relative to their mean values. The intrinsic diurnal cycle represented by the filled stars can easily be described as sinusoidal with a maximum in the morning hours and the minimum in the afternoon. The LWP mask contribution (open circles) has two maxima, in the morning and in the late afternoon with the minimum at midday. As pointed out before, the relative amplitude of the intrinsic fluctuation is greater than the macroscopic fluctuation of cloud cover in this region. This example demonstrates, that it is possible to distinguish between different sources of variability in overall LWP diurnal cycle when monitoring with SEVIRI. The analysis of the possible consequences on for example the energy budget or the transformation of cloud cover on longer time scales remains to be elucidated.

3.3 Seasonal variation

To complete the picture, the average diurnal cycle of low, middle level, high opaque and high semitransparent clouds in the Northern Hemisphere is displayed in Fig. 11. Contrary to the marine region considered before, the low clouds in here do not possess a pronounced morning maximum, a more striking feature is the second one around midday which is also the absolute maximum in the considered months.

The seasonal variation is present for all cloud types in the Northern Hemisphere. Predominantly a shifting of the curves can be detected. The highest mean values are found in October and the lowest in April in case of low clouds or middle level clouds. High semitransparent clouds show a maximum in July and a minimum in January. But not only the mean values fluctuate with time but also the shape of the diurnal cycle. High opaque clouds are variable in this respect, which indicates that the cloud formation mechanisms are complex and vary with time. The shape of the diurnal cycle of the other cloud classes is rather constant during the four seasons.

4 Conclusions

In this study we analysed the occurrence of LWP depending on cloud type. The objective was to find characteristic features of LWP for the individual cloud types. The general features of LWP, for example frequency distribution, average value and diurnal cycle are specified to serve as characteristic measures in atmospheric numerical modelling. With these measures, studies for a better description of LWP distribution in models under varying conditions as for example done by de Roode and Los (2008) are facilitated. Other possible applications are process studies or input data for cloud generators (Venema et al., 2006) and radiative transfer studies on a wide range of spatial scales. They can also provide verification in microphysical measurement experiments such as airborne probing of clouds.

Title Page

Abstract

Introduction

Conclusions

References

Tables

Figures



Back

Close

Full Screen / Esc

Printer-friendly Version

Interactive Discussion



LWP and CTY

A. Kniffka et al.

[Title Page](#)[Abstract](#)[Introduction](#)[Conclusions](#)[References](#)[Tables](#)[Figures](#)[Back](#)[Close](#)[Full Screen / Esc](#)[Printer-friendly Version](#)[Interactive Discussion](#)

Each cloud type possesses a characteristic average LWP distribution that is rather constant with time for the complete area observed by MSG, but variable for smaller regions, e.g. Europe. The fact, that the distributions do not change with time when considering the full disc shows that the disc is big enough to cover all cases for a cloud to be, so the statistics derived from such a large spatial field is robust and general for most applications. Also the two retrieval algorithms are independent enough, that one scheme does not limit the sample space of the other. LWP is derived by applying the Nakajima and King scheme using the 0.6 and 1.6 μm channels. The CTY algorithm does not use the 1.6 μm channel, but together with 6 other channels, the 0.6 μm channel is needed to distinguish high semitransparent or fractional clouds from the more opaque cloud types. However, for both thin cloud types several tests are applied which always include the two cases radiance of 0.6 μm below or above the same threshold. Hence the use of the 0.6 μm channel does not influence the frequency distribution of the individual cloud types. We studied the diurnal cycle of liquid water path for the entire year 2009 and found that also the diurnal cycle is dependent on cloud type. It has to be noted that clouds can develop during a day leading to a different type assignment by the retrieval. So clouds can change from one cloud type class into another, i.e. the diurnal cycle of LWP of a certain cloud type should be interpreted as being composed of the liquid water content averaged over all clouds of one type that are existing at the individual points in time.

The diurnal cycle of low clouds in the region of the coast of Angola and Namibia seems to be driven mainly by solar absorption. A numerical verification of cloud development through shortwave-heating via Large Eddy Simulation can be found in Chlond (2004). The diurnal cycle of middle level and high opaque clouds follows more a convective development, the clouds develop during a day and contain more liquid water in the afternoon. Please be aware that when considering the complete SEVIRI disc only a rough average is provided, which sums up all possible mechanisms of cloud development in just one curve per cloud type. Still we would consider these curves to be a useful approximation that can serve as prototype clouds in large scale numerical

LWP and CTY

A. Kniffka et al.

Title Page

Abstract

Introduction

Conclusions

References

Tables

Figures

◀

▶

◀

▶

Back

Close

Full Screen / Esc

Printer-friendly Version

Interactive Discussion



process studies or simulations on longer time scales because on the whole, the energy cycle or radiative cycle can be described correctly with these approximations. Another drawback is the typical problem of an imager mounted on a geostationary satellite: the cloud amount and also the liquid water path is dependent on the viewing geometry, and so the error increases towards the rims of the disc.

It is particularly noticeable that the relative amplitude of LWP's diurnal cycle can exceed that of CFC. This aspect needs further analysis and careful error assessment. Particularly the fluctuations of cloud optical thickness that result either from fluctuations of LWP or from CFC are of interest, to better quantify the absolute effect caused by fluctuations in the two quantities. Therewith the impact on radiative quantities such as heating rates or cloud radiative forcing will be assessed in future studies. In Wood et al. (2002) the normalised amplitude of the simultaneously retrieved low cloud amount is 50 % less than the LWP amplitude in subtropical regions. But shortwave radiative transfer calculations showed, that the cloud amount diurnal cycle has a 2–3 times larger influence on morning-afternoon differences in top of atmosphere shortwave radiative forcing. In this context, the impact of the diurnal variations of LWP and CFC should be considered in more detail.

In further analysis ice water path will be included, to investigate the effect of phase transition during the development of clouds, particularly convective cloud systems will be of interest.

Acknowledgements. This work was carried out within the framework of EUMETSAT's Satellite Application Facility on Climate Monitoring (CM SAF) in cooperation with the national meteorological institutes of Germany, Sweden, Finland, the Netherlands, Belgium, Switzerland, and the UK.

References

Ansmann, A., Tesche, M., Seifert, P., Althausen, D., Engelmann, R., Fruntke, J., Wandinger, U., Mattis, I., and Muller D.: Evolution of the ice phase in tropical altocumulus: SAMUM lidar

LWP and CTY

A. Kniffka et al.

Title Page

Abstract

Introduction

Conclusions

References

Tables

Figures

◀

▶

◀

▶

Back

Close

Full Screen / Esc

Printer-friendly Version

Interactive Discussion



observations over Cape Verde, *J. Geophys. Res.*, 114, D17208, doi:10.1029/2008JD011659, 2009.

Bony, S. and Dufresne, J.-L.: Marine boundary layer clouds at the heart of tropical cloud feedback uncertainties in climate models, *Geophys. Res. Lett.*, 32, L20806, doi:10.1029/2005GL023851, 2005.

Brunke, M. A., de Szoeko, S. P., Zuidema, P., and Zeng, X.: A comparison of ship and satellite measurements of cloud properties with global climate model simulations in the southeast Pacific stratus deck, *Atmos. Chem. Phys.*, 10, 6527–6536, doi:10.5194/acp-10-6527-2010, 2010.

Bugliaro, L., Zinner, T., Keil, C., Mayer, B., Hollmann, R., Reuter, M., and Thomas, W.: Validation of cloud property retrievals with simulated satellite radiances: a case study for SEVIRI, *Atmos. Chem. Phys.*, 11, 5603–5624, doi:10.5194/acp-11-5603-2011, 2011.

Chlond, A., Müller, F., and Sednev, I.: Numerical simulation of the diurnal cycle of marine stratocumulus during FIRE – A LES and SCM modeling study, *Q. J. Roy. Meteor. Soc.*, 130, 3297–3321, 2004.

Considine, G., Curry, J. A., and Wielicki, B.: Modeling cloud fraction and horizontal variability in marine boundary layer clouds, *J. Geophys. Res.*, 102, D12, 13517–13525, doi:10.1029/97JD00261, 1997.

Dee, D. P., Uppala, S. M., Simmons, A. J., Berrisford, P., Poli, P., Kobayashi, S., Andrae, U., Balmaseda, M. A., Balsamo, G., Bauer, P., Bechtold, P., Beljaars, A. C. M., van de Berg, L., Bidlot, J., Bormann, N., Delsol, C., Dragani, R., Fuentes, M., Geer, A. J., Haimberger, L., Healy, S. B., Hersbach, H., Hólm, E. V., Isaksen, I., Kållberg, P., Köhler, M., Matricardi, M., McNally, A. P., Monge-Sanz, B. M., Morcrette, J.-J., Park, B.-K., Peubey, C., de Rosnay, P., Tavolato, C., Thépaut, J.-N., and Vitart, F.: The ERA-Interim reanalysis: configuration and performance of the data assimilation system, *Q. J. Roy. Meteor. Soc.*, 137, 553–597, doi:10.1002/qj.828, 2011.

De Haan, J. F., Bosma, P., and Hovenier, J. W.: The adding method for multiple scattering calculations of polarized light, *Astron. Astrophys.*, 183, 371–391, 1987.

de la Torre Juárez, M., Davis, A. B., and Fetzer, E. J.: Scale-by-scale analysis of probability distributions for global MODIS-AQUA cloud properties: how the large scale signature of turbulence may impact statistical analyses of clouds, *Atmos. Chem. Phys.*, 11, 2893–2901, doi:10.5194/acp-11-2893-2011, 2011.

LWP and CTY

A. Kniffka et al.

Title Page

Abstract

Introduction

Conclusions

References

Tables

Figures

◀

▶

◀

▶

Back

Close

Full Screen / Esc

Printer-friendly Version

Interactive Discussion



Derrien, M.: Météo France/Centre de Meteorologie Spatiale: Algorithm Theoretical Basis Document for “Cloud Products” (CMA-PGE01 v3.0,CT-PGE02 v2.0 and CTTT-PGE03 v2.1), SAF/NWC/CDOP/MFL/SCI/ATBD/01, Version 3, Rev. 0, 2010.

Derrien, M. and Le Gléau, H.: MSG/SEVIRI cloud mask and type from SAFNWC, *Int. J. Remote Sens.*, 26, 4707–4732, 2005.

Derrien, M. and Le Gléau, H.: Improvement of cloud detection near sunrise and sunset by temporal differencing and region-growing techniques with real-time SEVIRI, *Int. J. Remote Sens.*, 31, 1765–1780, 2010.

de Roode, S. and Los, A.: The effect of temperature and humidity fluctuations on the liquid water path of non-precipitating closed-cell stratocumulus clouds, *Q. J. Roy. Meteor. Soc.*, 134, 403–416, doi:10.1002/qj.222, 2008.

EUMETSAT: A Planned Change to the MSG Level 1.5 Image Product Radiance Definition, EUM/OPS-MSG/TEN/06/0519, 2007.

EUMETSAT: MSG Level 1.5 Image Data Format Description, EUM/MSG/ICD/105 v6, 2010.

Hannay, C., Williamson, D. L., Hack, J. J., Kiehl, J. T., Olson, J. G., Klein, S. A., Bretherton, C. S., and Kohler, M.: Evaluation of Forecasted Southeast Pacific Stratocumulus in the NCAR, GFDL, and ECMWF Models, *J. Climate*, 22, 2871–2889, doi:10.1175/2008JCLI2479.1, 2009.

Hollmann, R.: Annual Product Quality Assessment Report 2010, SAF/CM/DWD/VAL/OR6, Version 1.1, 2011.

Hu, Y., Rodier, S., Xu, K., Sun, W., Huang, J., Lin, B., Zhai, P., and Josset, D.: Occurrence, liquid water content, and fraction of supercooled water clouds from combined CALIOP/IIR/MODIS measurements, *J. Geophys. Res.*, 115, D00H34, doi:10.1029/2009JD012384, 2010.

Jiang, J. H., Su, H., Zhai, C., Perun, V. S., Del Genio, A., Nazarenko, L. S., Donner, L. J., Horowitz, L., Seman, C., Cole, J., Gettelman, A., Ringer, M. A., Rotstain, L., Jeffrey, S., Wu, T. W., Briant, F., Dufresne, J. L., Kawai, H., Koshiro, T., Watanabe, M., L’Ecuyer, T. S., Volodin, E. M., Iversen, T., Drange, H., Mesquita, M. D. S., Read, W. G., Waters, J. W., Tian, B. J., Teixeira, J., and Stephens, G. L.: Evaluation of cloud and water vapor simulations in CMIP5 climate models using NASA “A-Train” satellite observations, *J. Geophys. Res.*, 117, D14105, doi:10.1029/2011JD017237, 2012.

Kniffka, A., Meirink, J. F., Stengel, M.: Algorithm Theoretical Basis Document SEVIRI cloud products Edition 1, SAF/CM/DWD/ATBD/SEV/CLD, Version 1.1, 2013a.

LWP and CTY

A. Kniffka et al.

Title Page

Abstract

Introduction

Conclusions

References

Tables

Figures

◀

▶

◀

▶

Back

Close

Full Screen / Esc

Printer-friendly Version

Interactive Discussion



- Kniffka, A., Lockhoff, M., Stengel, M., Meirink, J. F.: Validation Report SEVIRI cloud products Edition 1, SAF/CM/DWD/VAL/SEV/CLD, Version 1.1, 2013b.
- Korolev, A. and Isaac, G.: Phase transformation of mixed-phase clouds, *Q. J. Roy. Meteor. Soc.*, 129, 19–38, 2003.
- 5 McBride, P. J., Schmidt, K. S., Pilewskie, P., Walther, A., Heidinger, A. K., Wolfe, D. E., Fairall, C. W., and Lance, S.: CalNex cloud properties retrieved from a ship-based spectrometer and comparisons with satellite and aircraft retrieved cloud properties, *J. Geophys. Res.*, 117, D00V23, doi:10.1029/2012JD017624, 2012.
- Meirink, J. F., Roebeling, R. A., and Stammes, P.: Inter-calibration of polar imager solar channels using SEVIRI, *Atmos. Meas. Tech. Discuss.*, 6, 3215–3247, doi:10.5194/amtd-6-3215-2013, 2013a.
- 10 Meirink, J. F., Kniffka, A., Lockhoff, M., and Stengel, M.: Evaluation of cloud optical and microphysical property observations in the CLAAS dataset, *Atmos. Chem. Phys. Discuss.*, in preparation, 2013b.
- 15 O'Dell, C., Wentz, F., and Bennartz, R.: Cloud liquid water path from satellite-based passive microwave observations: a new climatology over the global oceans, *J. Climate*, 21, 1721–1739, 2008.
- Pfeifroth, U.: Tagesgang von Bewölkung in satellitenbasierten und synoptischen Beobachtungen sowie in regionalen Klimasimulationen, Institut für Atmosphäre und Umwelt, Goethe-Universität Frankfurt, 2009.
- 20 Roebeling, R. A., Feijt, A. J., and Stammes, P.: Cloud property retrievals for climate monitoring: implications of differences between Spinning Enhanced Visible and Infrared Imager (SEVIRI) on Meteosat-8 and Advanced Very High Resolution Radiometer (AVHRR) on NOAA-17, *J. Geophys. Res.*, 111, D20210, doi:10.1029/2005JD006990, 2006.
- 25 Roebeling, R. A., Deneke, H. M., and Feijt, A. J.: Validation of cloud liquid water path retrievals from SEVIRI using one year of CloudNET observations, *J. Appl. Meteorol. Clim.*, 47, 206–222, 2008.
- Rossow, W. B. and Schiffer, R. A.: Advances in understanding clouds from ISCCP, *B. Am. Meteorol. Soc.*, 80, 2261–2287, 1999.
- 30 Schulz, J., Albert, P., Behr, H.-D., Caprion, D., Deneke, H., Dewitte, S., Dürr, B., Fuchs, P., Gratzki, A., Hechler, P., Hollmann, R., Johnston, S., Karlsson, K.-G., Manninen, T., Müller, R., Reuter, M., Riihelä, A., Roebeling, R., Selbach, N., Tetzlaff, A., Thomas, W., Werscheck, M., Wolters, E., and Zelenka, A.: Operational climate monitoring from space: the EUMETSAT

[Title Page](#)[Abstract](#)[Introduction](#)[Conclusions](#)[References](#)[Tables](#)[Figures](#)[◀](#)[▶](#)[◀](#)[▶](#)[Back](#)[Close](#)[Full Screen / Esc](#)[Printer-friendly Version](#)[Interactive Discussion](#)

Satellite Application Facility on Climate Monitoring (CM-SAF), Atmos. Chem. Phys., 9, 1687–1709, doi:10.5194/acp-9-1687-2009, 2009.

Schmetz, J., Pili, P., Tjemkes, S., Just, D., Kerkmann, J., Rota, S., and Ratier, A.: An introduction to Meteosat Second Generation (MSG), B. Am. Meteorol. Soc., 83, 977–992, 2002.

5 Seethala, C. and Horvath, A.: Global assessment of AMSR-E and MODIS cloud liquid water path retrievals in warm oceanic clouds, J. Geophys. Res., 115, D13202, doi:10.1029/2009JD012662, 2010.

Stammes, P.: Spectral radiance modeling in the UV-Visible range, in: IRS 2000: Current Problems in Atmospheric Radiation, edited by: Smith, W. L. and Timofeyev, Y. M., A. Deepak Publ., Hampton, Va., 385–388, 2001.

10 Stengel, M., Kniffka, A., Fokke Meirink, J., Lockhoff, M., and Tan, J.: CLAAS: the CMSAF cloud property dataset using SEVIRI, Atmos. Chem. Phys. Discuss., accepted, 2013b.

Stephens, G. L.: Radiation profiles in extended water clouds: II. Parameterization schemes, J. Atmos. Sci., 35, 2123–2132, 1978.

15 Stubenrauch, C., Kinne, S., and the GEWEX Cloud Assessment Team: Assessment of global cloud climatologies, GEWEX WCRP Global Energy and Water Cycle Experiment News, 19, 6–7, 2009.

20 Turner, D. D., Vogelmann, A. M., Austin, R. T., Barnard, J. C., Cady-Pereira, K., Chiu, J. C., Clough, S. A., Flynn, C., Khaiyer, M. M., Liljegren, J., Johnson, K., Lin, B., Long, C., Marshak, A., Matrosov, S. Y., McFarlane, S. A., Miller, M., Min, Q., Minnis, F., O’Hirok, W., Wang, Z., and Wiscombe, W.: Thin liquid water clouds: their importance and our challenge, B. Am. Meteorol. Soc., 88, 2, 177–190, doi:10.1175/BAMS-88-2-177, 2007.

Venema V., Meyer, S., Gimeno García, S., Kniffka, A., Simmer, C., Crewell, S., Loehnert, U., Trautmann, T., and Macke, A.: Surrogate cloud fields generated with the Iterative Amplitude Adapted Fourier Transform algorithm, Tellus, 58A, 104–120, 2006.

25 Williams, K. D. and Webb, M. J.: A quantitative performance assessment of cloud regimes in climate models, Clim. Dynam., 33, 1, 141–157, doi:10.1007/s00382-008-0443-1, 2008.

Wood, R. and Hartmann, D. L.: Spatial variability of liquid water path in marine low cloud: the importance of mesoscale cellular convection, J. Climate, 19, 1748–1764, 2006.

30 Wood, R., Bretherton, C. S., and Hartmann, D. L.: Diurnal cycle of liquid water path over the subtropical and tropical oceans, Geophys. Res. Lett., 29, 2092, doi:10.1029/2002GL015371, 2002.

LWP and CTY

A. Kniffka et al.

Title Page

Abstract

Introduction

Conclusions

References

Tables

Figures

◀

▶

◀

▶

Back

Close

Full Screen / Esc

Printer-friendly Version

Interactive Discussion



Table 1. Cloud types of CM SAF CTY parameter and corresponding pressure levels, see Derrien et al. (2010).

Cloud Type	p
Very low opaque clouds	$p > 800$ hPa
Low opaque clouds	$650 \text{ hPa} < p \leq 800$ hPa
Medium opaque clouds	$450 \text{ hPa} < p \leq 650$ hPa
High opaque clouds	$300 \text{ hPa} < p \leq 450$ hPa
Very high opaque clouds	$p \leq 300$ hPa

LWP and CTY

A. Kniffka et al.

Title Page

Abstract

Introduction

Conclusions

References

Tables

Figures

I◀

▶I

◀

▶

Back

Close

Full Screen / Esc

Printer-friendly Version

Interactive Discussion



Table 2. Average LWP (g m^{-2}) for land and water pixel on the SEVIRI disc for January, April, July and October 2009, only filled pixel were averaged.

	Low	middle level	high opaque	high semi.	fractional
Land					
Average values					
Jan	98.8	199.8	206.0	41.1	8.9
Apr	78.4	181.5	202.2	37.4	9.3
Jul	79.3	161.2	239.4	39.0	9.2
Oct	108.6	215.3	234.7	50.1	9.6
Variances					
Jan	27.5	53.7	48.7	12.0	2.9
Apr	23.6	48.7	42.3	11.7	2.7
Jul	26.2	52.4	41.7	12.6	3.0
Oct	27.4	53.6	44.8	12.5	3.0
Water					
Average values					
Jan	84.0	139.4	140.3	40.6	6.7
Apr	65.4	141.6	176.5	29.5	6.3
Jul	63.4	143.4	154.3	32.5	5.8
Oct	79.2	150.8	149.4	37.2	6.3
Variances					
Jan	27.4	52.6	48.8	14.9	2.4
Apr	19.7	46.0	44.8	8.9	1.9
Jul	19.5	49.4	40.2	11.0	1.9
Oct	22.5	47.3	42.4	10.8	2.0

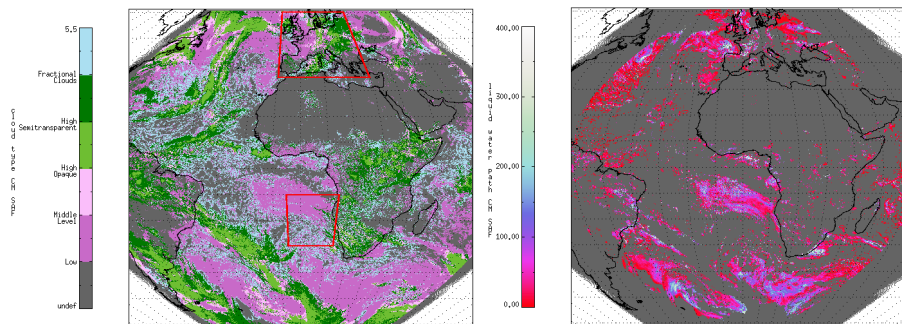


Fig. 1. Left: cloud type for liquid and ice pixel on full SEVIRI disc with horizontal resolution $3\text{ km} \times 3\text{ km}$ at subsatellite point, the red squares depict the two regions of interest, right: liquid water path; both at 11:45 UTC, 10 October 2009.

[Title Page](#)[Abstract](#)[Introduction](#)[Conclusions](#)[References](#)[Tables](#)[Figures](#)[◀](#)[▶](#)[◀](#)[▶](#)[Back](#)[Close](#)[Full Screen / Esc](#)[Printer-friendly Version](#)[Interactive Discussion](#)

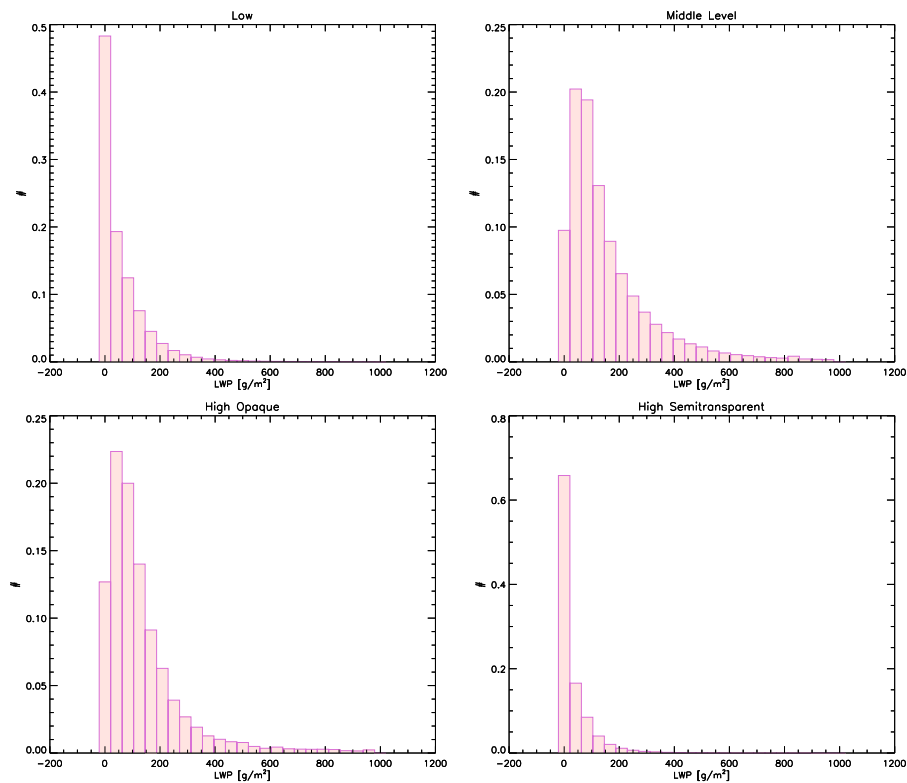
[Title Page](#)[Abstract](#)[Introduction](#)[Conclusions](#)[References](#)[Tables](#)[Figures](#)[⏪](#)[⏩](#)[◀](#)[▶](#)[Back](#)[Close](#)[Full Screen / Esc](#)[Printer-friendly Version](#)[Interactive Discussion](#)

Fig. 2. Frequency distribution of LWP for 4 cloud types, average for 7 October 2009. Upper left: low clouds, upper right: middle level, middle left: high opaque, middle right: high semitransparent.

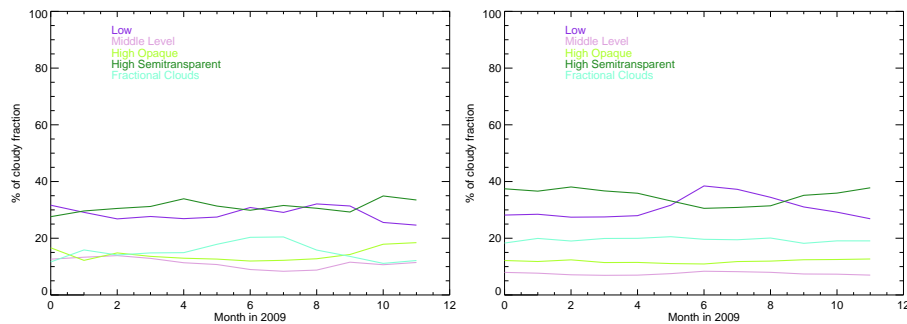


Fig. 3. Averaged proportion of cloud types from the cloudy fraction in 2009 based on monthly mean data, left: Europe; right: SEVIRI disc.

[Title Page](#)
[Abstract](#)
[Introduction](#)
[Conclusions](#)
[References](#)
[Tables](#)
[Figures](#)
[⏪](#)
[⏩](#)
[◀](#)
[▶](#)
[Back](#)
[Close](#)
[Full Screen / Esc](#)
[Printer-friendly Version](#)
[Interactive Discussion](#)


LWP and CTY

A. Kniffka et al.

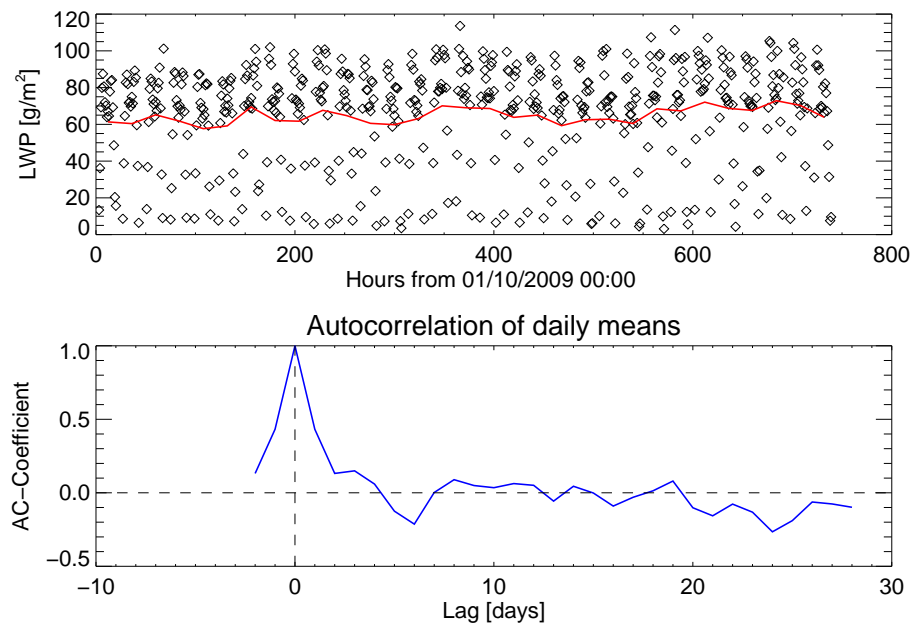


Fig. 4. Upper panel: time series of LWP for low clouds in Europe, October 2009, the red line shows the daily averages, diamonds depict spatial averages of the individual time slots; lower panel: auto-correlation function of daily averaged data.

[Title Page](#)[Abstract](#)[Introduction](#)[Conclusions](#)[References](#)[Tables](#)[Figures](#)[◀](#)[▶](#)[◀](#)[▶](#)[Back](#)[Close](#)[Full Screen / Esc](#)[Printer-friendly Version](#)[Interactive Discussion](#)

LWP and CTY

A. Kniffka et al.

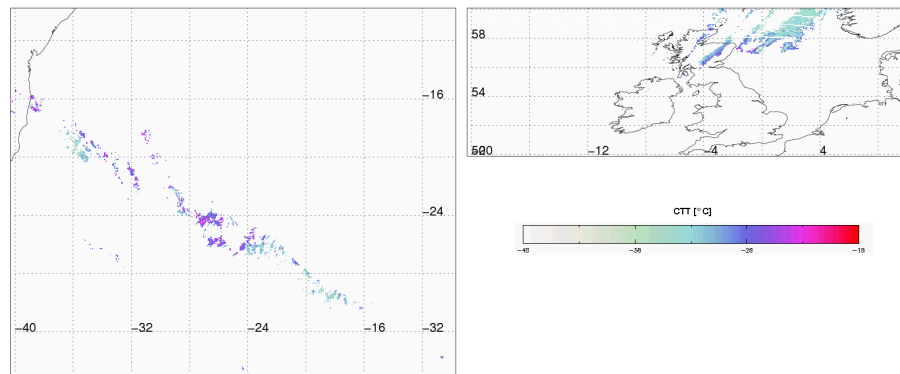


Fig. 5. High opaque clouds with liquid water on top, left: over ocean (10 October 2009, 11.45 a.m.), right: British Isles land and ocean (20 October 2009, 11.45 a.m.), only pixel with $CTT > -38^{\circ}\text{C}$.

[Title Page](#)[Abstract](#)[Introduction](#)[Conclusions](#)[References](#)[Tables](#)[Figures](#)[◀](#)[▶](#)[◀](#)[▶](#)[Back](#)[Close](#)[Full Screen / Esc](#)[Printer-friendly Version](#)[Interactive Discussion](#)

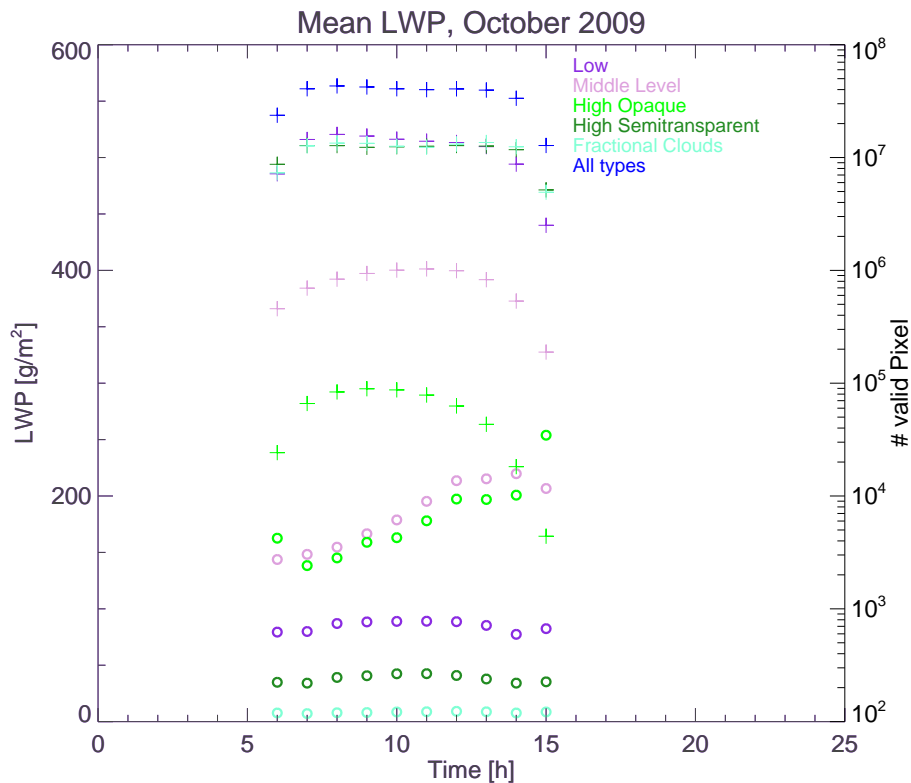


Fig. 6. Average diurnal cycle of LWP for distinct cloud types (circles) and the corresponding number of occurrence (plus signs) October 2009. Level 2 data from the Northern Hemisphere of SEVIRI disc were considered.

LWP and CTY

A. Kniffka et al.

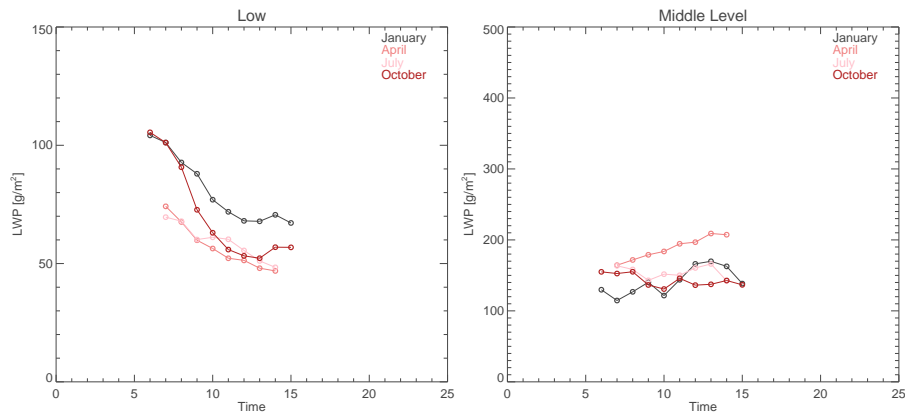


Fig. 7. Average diurnal cycle of LWP for 4 months in 2009 for the cloud deck off the coast of Namibia and Angola, left: low clouds, right, middle level clouds. Cloud-free pixel were not included.

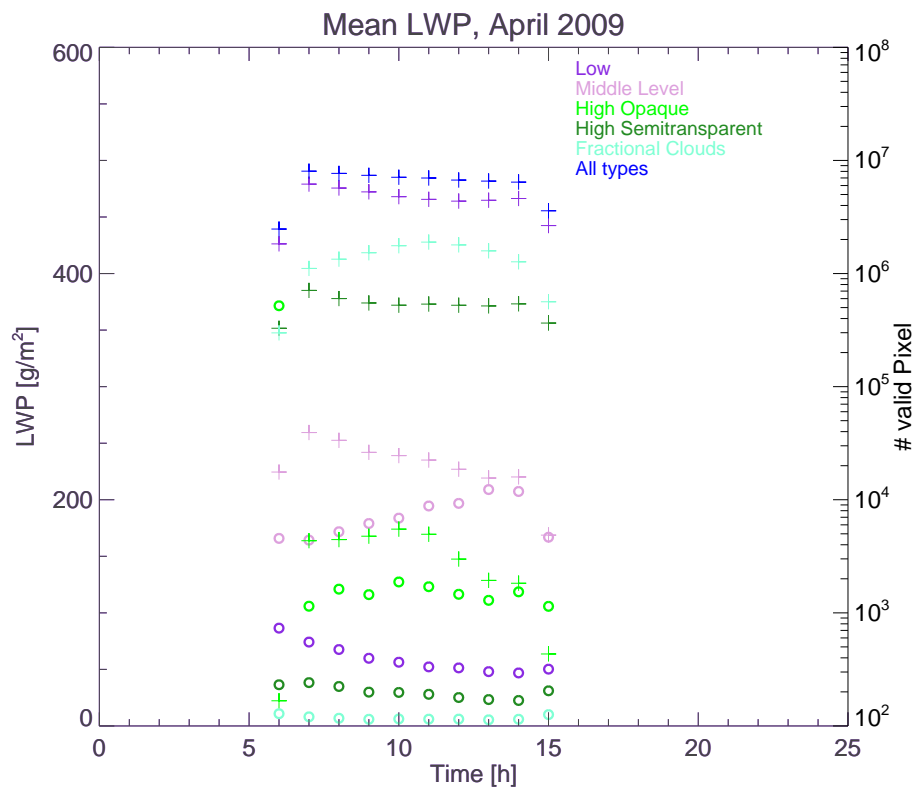


Fig. 8. Circles: average diurnal cycle of LWP for distinct cloud types in the cloud deck off the coast of Namibia and Angola, April 2009; plus signs: corresponding number of observations.

Title Page

Abstract Introduction

Conclusions References

Tables Figures

◀ ▶

◀ ▶

Back Close

Full Screen / Esc

Printer-friendly Version

Interactive Discussion



LWP and CTY

A. Kniffka et al.

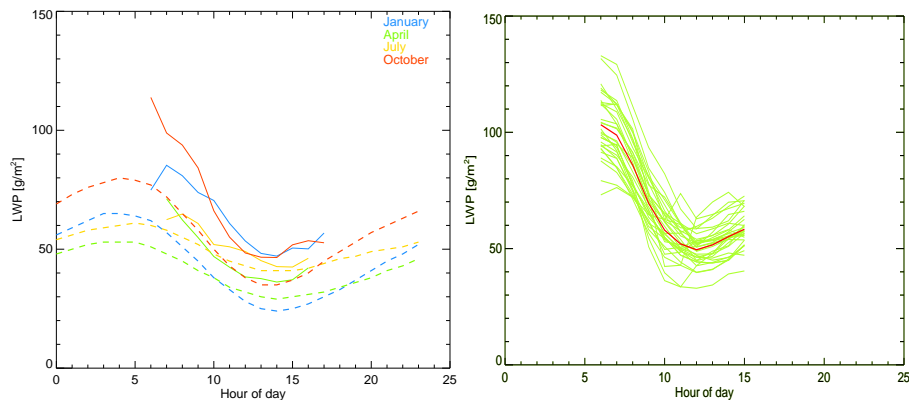


Fig. 9. Left: average diurnal cycle of LWP for 4 months in 2009 from SEVIRI (solid lines) compared to climatological values of 1988–2008 derived from microwave measurements (dashed lines), all cloud types. Right: individual diurnal cycles for October 2009 as seen from SEVIRI, also cloud-free pixels were included in the average for consistency with the microwave LWP climatology.

[Title Page](#)[Abstract](#)[Introduction](#)[Conclusions](#)[References](#)[Tables](#)[Figures](#)[⏪](#)[⏩](#)[◀](#)[▶](#)[Back](#)[Close](#)[Full Screen / Esc](#)[Printer-friendly Version](#)[Interactive Discussion](#)

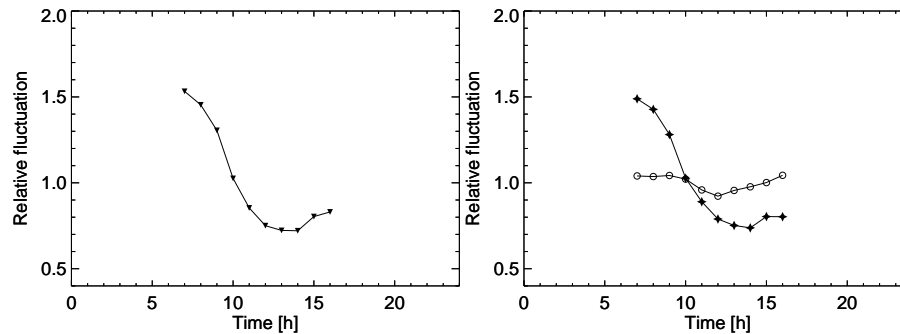


Fig. 10. Left: relative diurnal cycle of LWP of all clouds for October 2009 as seen from SEVIRI. Right: relative diurnal cycle splitted into the intrinsic variability of LWP (black stars) and the variability caused by cloud fraction fluctuation.

[Title Page](#)[Abstract](#)[Introduction](#)[Conclusions](#)[References](#)[Tables](#)[Figures](#)[◀](#)[▶](#)[◀](#)[▶](#)[Back](#)[Close](#)[Full Screen / Esc](#)[Printer-friendly Version](#)[Interactive Discussion](#)

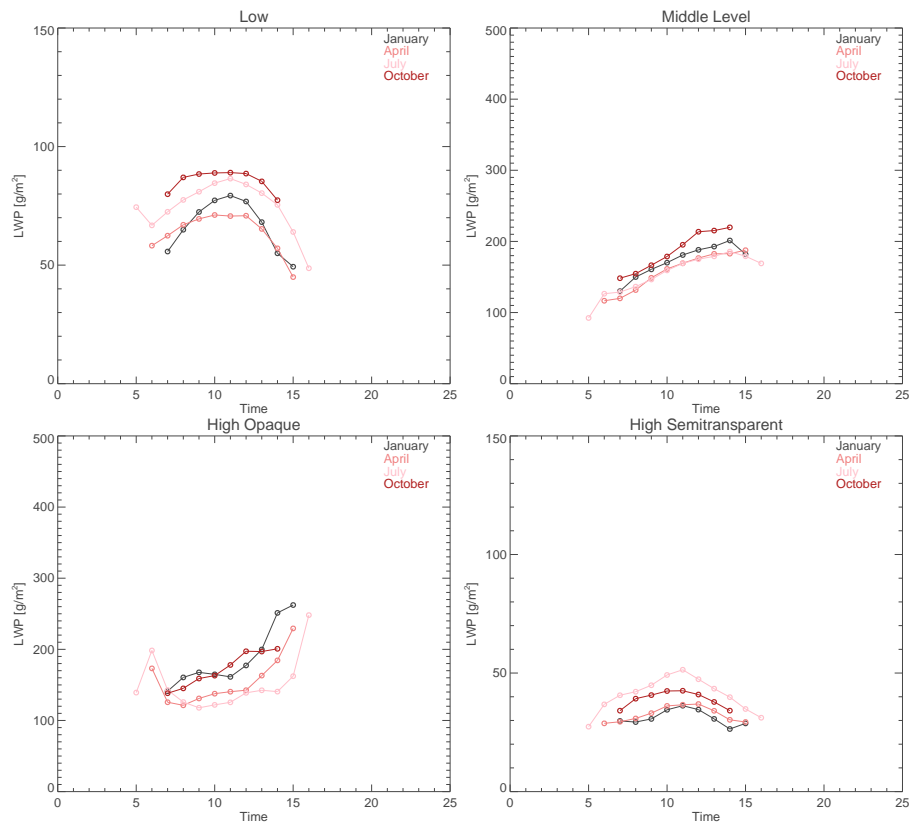


Fig. 11. Average diurnal cycle of LWP for 4 months in 2009 for the Northern Hemisphere in the MSG disc, left: low clouds, right, middle level clouds. Cloud-free pixel were not averaged.